



Scholars Research Library

Der Pharma Chemica, 2015, 7(12):264-274
(<http://derpharmachemica.com/archive.html>)



ISSN 0975-413X
CODEN (USA): PCHHAX

Comparison between photo catalytic activity of pure ZnO and silver ion doped ZnO For decomposition of Methyl Green (MG) dye from wastewater

Ahmed A. Abdel-Khalek^a, Hossam F. Nassar^b, Fagr Kh. Abdel-Gawad^b and Afaf Hashem^a

^aChemistry Department, Faculty of Science, Beni-Suef University, Beni-Suef City, Egypt

^bWater Pollution Control Department, Environmental Research Division, National research Center, El-Dokki, Cairo, Egypt

ABSTRACT

Developing hygienically advanced water treatment technologies is a must as a result of environmental pollution and industrialization. Currently used water treatment technique requires high costs and well equipped laboratories. Efficient water treatment imposes conversion of hazardous substances to safe ones in addition to evolution of efficient risk management approaches from dangerous effects of pollutants which are toxic, everlasting and laborious to be treated. The present work represents a method for treatment, deterioration and decolorization of methyl green (MG) in wastewater using both pure ZnO and Ag⁺ doped ZnO under UV- Visible light. The photodegradation processes of dye have been studied using UV-Vis spectrophotometry. The parameters studied were the initial pH values using NaOH and H₂SO₄, amount of catalyst, initial dye concentration, and the presence of NaCl, and Na₂SO₄. The effect of pure ZnO as catalyst has been compared with Ag⁺ doped ZnO catalyst. The optimum conditions had been determined, and found the efficiency of degradation for both catalyst. From results found the dye degradation was more efficient in case of Ag⁺ doped ZnO than pure ZnO.

Key words: Methyl Green (MG) dye, Photocatalytic activity, waste water treatment, ZnO and ZnO doped Ag ion

INTRODUCTION

Water can be considered a vital constituent in many life activities; domestic, agricultural and industrial. Drain water resulted from different human activities usually encounters bulk of contaminants. Water pollution by toxic organic compounds is a topic of worldwide concern[1-4]. Wastewater also is intensely dyed, polluted with high concentration of organic materials such as; suspended and dissolved salts in addition to other recalcitrant compounds. A major encouraging technique used nowadays among many oxidation processes (AOPS) is heterogeneous photocatalysis, it may be used effectively for organic pollutants degradation in water. Where, during textile and dyestuff industries, about (10–15%) of all dyes are released instantly as crude dye in the wastewater effluents and their ejection into water streams is very dangerous to environment health [5]. Dyes are classified as anionic (direct, acid and reactive dyes); cationic (basic dyes); and nonionic (disperse dyes). They usually have complex aromatic molecular structures and are classified according to their chromophore (component of the molecule that is responsible for color) such as azo, anthraquinone, arylmethane, acridine, triphenylmethane, heterocyclic, cyanine, phthal- ocyanine, nitro, nitroso, quinone-imine, thiazole or xanthene dyes [4-7]. Cationic triphenylmethane dyes are widely used as colorants in industry and also as antimicrobial advocates [8]. Methyl green (MG) is a basic triphenylmethane-type dicationic dye, commonly used in staining solutions in medicine and biology [8].

There are many techniques used in wastewater treatment for removal of dyes such as: incineration, biological treatment, ozonation and adsorption on solid phases. However, these techniques have some drawbacks, for example hazardous volatiles result from incineration. Biological treatment needs a lot of time and results in bad odors.

Ozonization produces short half life, ozone persistence is influenced by salts presence, pH, temperature and the absorption presents phase transmission of pollutant, not degrading it and producing sludge [10-12]. By this way, the diversified photocatalysis becomes a suitable alternative to dye decomposition. This technique has many advantages over others concerning dye degradation to final products [4,14].

Recently, an alternative to non-destructive methods is "advanced oxidation processes" (AOPs), based on the generation of very reactive species such as hydroxyl radicals that quickly and non-selectively oxidizes a broad range of organic pollutants [15–18]. AOPs include photocatalysis systems such as combination of a semiconductor (TiO₂, ZnO Fe₂O₃, etc.) and UV light. Semiconductors are important due to their electronic structure of the metal atoms in chemical combination, which is characterized by a filled valence band and an empty conduction band [4,19]. As one of the most important II-VI semiconductors, ZnO with a wide band gap of 3.37 eV is an environmentally friendly and chemically stable material and is also an ideal photocatalyst besides TiO₂. In some cases, ZnO exhibits better degradation capacity than TiO₂[20-23].The biggest advantage of ZnO compared with TiO₂ is that it absorbs a larger fraction of the UV spectrum and more light quanta [24].The rapid recombination of electron-hole pair also limits the efficiency of TiO. Higher photocatalytic efficiency of ZnO compared to TiO₂ has been reported especially for degradation of organics in aqueous solutions [25,26].

The photocatalytic activity of ZnO can be improved by various techniques such as by an increase of surface area [26], control of the designed shape [25], incorporating another atom into the lattice causes separation of electron-hole pairs [29,30]. Ag⁺doped ZnO particles improving photocatalytic activities because Ag acting as electron sinks can trap the photoexcited electrons from the semiconductor and inhibiting the charge recombination process [31,32]and thus improve the separation efficiency of photoexcited electrons and holes,which leads to improvement of photocatalytic efficiency of ZnO.

The photocatalytic degradation follows a pseudo-first order reaction and its kinetics can be expressed using $\ln(C_0/C_t) = kt$, where k is the apparent reaction rate constant, C₀ the initial concentration of MG, the reaction time and C_t is the concentration of MG at the reaction time t [33].

The degradation efficiency is calculated using the following equation:

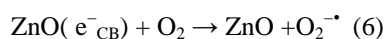
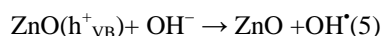
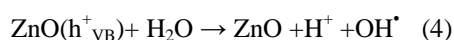
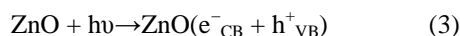
$$\text{Degradation rate(\%)} = \frac{C_0 - C_t}{C_0} * 100\% \quad (1)$$

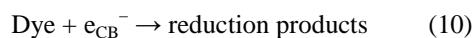
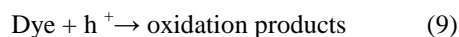
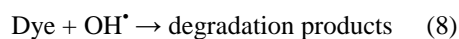
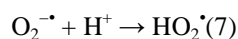
$$= \frac{A_0 - A_t}{A_0} * 100\% \quad (2)$$

where C₀ represents the initial concentration, C_t the variable concentration at time t, A₀ the initial absorbance, and A_t the variable absorbance at time t.

MECHANISMS OF PHOTOCATALYSIS

Photocatalysis may be termed as a photo-induced reaction which is accelerated by the presence of a catalyst. These types of reactions are activated by absorption of a photon with sufficient energy (equals or higher than the band-gap energy (E_{bg}) of the catalyst) [4,35]. The absorption leads to a charge separation due to promotion of an electron (e⁻) from the valence band of the semiconductor catalyst to the conduction band, thus generating a hole (h⁺) in the valence band. The recombination of the electron and the hole must be prevented as much as possible if a photocatalyzed reaction must be favored. The reaction between the activated electrons with an oxidant to produce a reduced product, and also a reaction between the generated holes with a reductant to produce an oxidized product. The photogenerated electrons could reduce the dye or react with electron acceptors such as O₂ adsorbed on the Zn(II)-surface or dissolved in water, reducing it to superoxide radical anion O₂^{-•} [36]. The photogenerated holes can oxidize the organic molecule to form R⁺, or react with OH⁻ or H₂O oxidizing them into OH[•] radicals. Together with other highly oxidant species (peroxide radicals) they are reported to be responsible for the heterogeneous ZnO photodecomposition of organic substrates as dyes. The resulting OH[•] radical, being a very strong oxidizing agent (standard redox potential +2.8V) can oxidize most dyes to the mineral end-products. According to this, the relevant reactions at the semiconductor surface causing the degradation of dyes can be expressed as follows [36]:





Where $h\nu$ is photon energy required to excite the semiconductor electron from the valence band (VB) region to conduction band (CB) region.

MATERIALS AND METHODS

3.1. Materials

All chemicals were used in the as-received condition without any further purification.

Methyl Green (*Sigma-Aldrich*). Linear Formula $\text{C}_{27}\text{H}_{35}\text{BrClN}_3 \cdot \text{ZnCl}_2$. Molecular Weight (653.24) Color Index Number 42590 CAS Number 7114-03-6. **IUPAC:** 4-[[4-(dimethylamino)phenyl][4-(dimethyliminiumyl)cyclohexa-2,5-dien-1-ylidene]methyl]-N-ethyl-N,N-dimethylanilinium bromide chloride

Zinc sulfat-7-hydrat ($\text{Zn}(\text{SO}_4) \cdot 7\text{H}_2\text{O}$) (Riedel), **Sodium Carbonate anhydrouse** (Na_2CO_3), **Silver Nitrate** (AgNO_3), **NaOH**, **H_2SO_4** , **NaCl**, **Na_2SO_4** and **Ethanol** were purchased from Merck and were of analytical reagent grade.

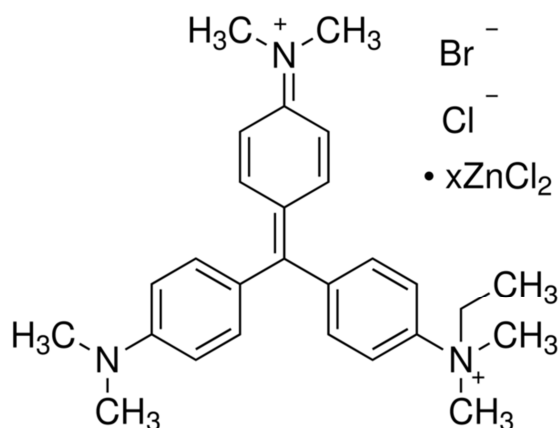


Fig.1. Structure of methyl green

3.2. Preparation of photocatalysts

Preparation of Ag^+ doped ZnO by Precipitation method. $\text{Zn}(\text{SO}_4) \cdot 7\text{H}_2\text{O}$ and Na_2CO_3 are dissolved separately in double distilled water to get 0.5 mol/l solutions. Zinc sulfat solution is slowly added into vigorously stirred Na_2CO_3 . AgNO_3 in the required stoichiometry was added bit by bit into the above solution and gray precipitate was detected. The precipitate was then filtered, rinsed many times with distilled water, and then washed twice with ethanol. The resultant solid product was dried at 100°C for 12 h and calcined at $600(\pm 2)^\circ\text{C}$ for 2 h. ZnO particle could be also prepared by the same procedure without using AgNO_3 solution [33].

3.3. Preparation of stock solution

Weight ~ 0.05 g of Methyl Green into a 50 ml beaker. Dissolve the dye in double distilled water and transfer it to a 1 L volumetric flask.

3.4. Catalyst Characterization

Fig. 2 displays the XRD patterns of undoped ZnO and Ag^+ doped ZnO samples. They reveal the crystal structures of the undoped as well as the doped oxides as primitive hexagonal wurtzite structure (space group $\text{P6}_3\text{mc}$ (186) [5, 6]) with two zinc and two oxygen atoms per unit cell. The hexagonal wurtzite structure, the strong peak intensity and the small line width imply the good crystallinity [7, 8]. The XRD of Ag^+ doped ZnO does not display peaks of metallic Ag at 38.1° (111), 44.3° (200), etc., (JCPDS 89-3722). This may be because of the low content of Ag. Silver is unlikely to be present as Ag_2O in the prepared Ag^+ doped ZnO . The doped oxide has been calcined at 600°C where as Ag_2O decomposes to Ag at 400°C . Moreover, at annealing temperature greater than 600°C , the silver dopants diffuse out

partially and form silver clusters. Contrarily, with annealed temperature ≥ 600 °C, there is not any peak attributed to Ag could be observed. That may indicate that the substitution for Zn atom sites by Ag ions is instable at high temperature, which might be a limitation for silver as the dopant of ZnO[6].

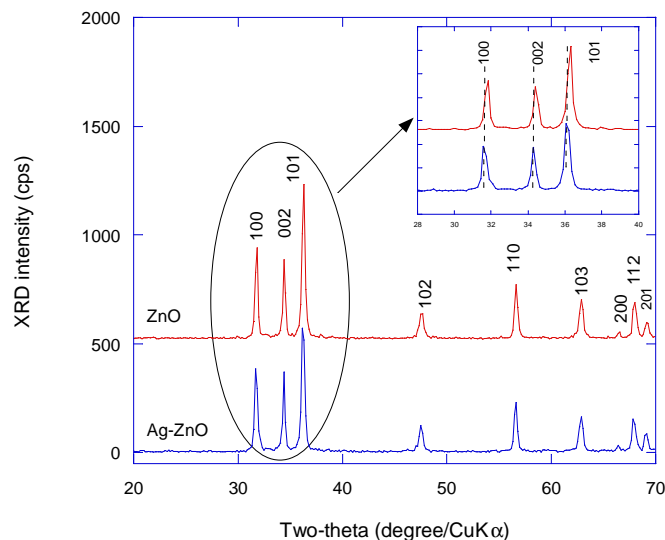


Fig.3. XRD pattern of ZnO and Ag⁺doped ZnO oxides. Bragg lines are indexed in the P6_{3mc} space group with the hexagonal sitting. Insert shows detail in the range $2\theta = 28-40^\circ$

Silver may be incorporated in ZnO lattice either at interstitials or as substituent for Zn²⁺ [10].

Table.1 shows the results of the structural analysis of ZnO and Ag⁺doped ZnO powders. Unit-cell parameters were calculated via a least squares refinement method using 9 well-defined diffraction lines with indexation in the hexagonal system. As shown in Tab.1, replacement of Zn by Ag produces slight changes of the lattice parameters; the *a*-axis enlarged and the *c*-axis shrinks; consequently, the unit cell volume increased by 1.5% for Ag⁺doped ZnO sample. It is attributed to the substitution of Zn²⁺ ions (radius of 0.74 Å) by Ag⁺ ions (radius of 1.26 Å) [11]. We can demonstrate that their values are close to but slightly deviated from those of pure ZnO, which indicated the Ag ions successfully occupied the lattice site rather than interstitial ones. Moreover, the formation energy is very low for Ag ions on the substitutional sites, but rather high at the interstitial sites. Thus, Ag ions prefer to occupy substitutional sites [4,12]. It is interesting to remark that the lattice parameter variations are very similar for the different dopants [13]. It is also important to note that the peaks of the as-sintered Ag⁺doped ZnO samples shifted towards lower angles (the inserted portions in Fig.2 of XRD patterns (in the $2\theta = 28-40^\circ$) ZnO and Ag⁺doped ZnO illustrating the lattice parameter shifts in the solid solution), this peak shifting and broadening may be attributed to the lattice mismatching, lattice distortion, strain of the crystal, and the finite size effect.

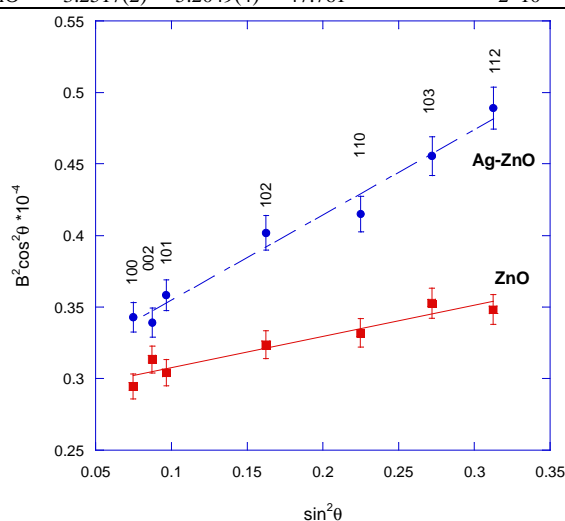
In general, several factors can contribute to the broadening of peaks in X-ray diffraction [14, 15]. For example, the instrumental factors related to the resolution and the incident X-ray wavelength, as well as the sample factors such as crystallite size and non-uniform microstrain, can cause a line broadening. In the case of an instrumental broadening, the line width will vary smoothly with 2θ or *d* spacing. On the other hand, the line broadening originating from the sample characteristics will have a different relationship. By combining the Scherrer's equation for crystallite size and the Bragg's law for diffraction, crystallite size and microstrain components are estimated by using the following equation.

$$B^2 \cos^2 \theta = 16 \langle e^2 \rangle \sin^2 \theta + \frac{K^2 \lambda^2}{L^2} \quad (11)$$

where *B* is the full-width at half-maximum (FWHM) after correction of the instrumental broadening for finely powdered silicon powder, θ is the diffraction angle, and *K* is a near-unity constant related to crystallite shape. The plot of the first member as a function of $\sin^2 \theta$ is reported in Fig. 3 for the pristine ZnO and its Ag doped ZnO. The plots are well fit by straightlines, in agreement with Eq. (11). The slope of the linear fit of the data provides us with the value of $\langle e^2 \rangle$, while the extrapolation to $\sin^2 \theta = 0$ provides us with the value of the coherence length *L*. Apparently, the integral breadth of Bragg lines of the Ag doped ZnO is slightly greater than undoped ZnO, which suggests a smaller grain size and higher microstrain content Table.1.

Table.1 Lattice parameters of undoped ZnO and Ag⁺ doped ZnO powders calculated using the wurtzite structure (P6_{3mc} S.G.)

Samples	Lattice parameters		Unit-cell volume(Å ³)	Stain (e)	L(nm)
	a(Å)	c(Å)			
Reference	3.250	5.207	[.63	----	----
ZnO	3.248(4)	5.2079(7)	47.538	1*10 ⁻³	28
Ag-ZnO	3.2517(2)	5.2049(4)	47.761	2*10 ⁻³	20

**Fig.3.** Analysis of the full-width B at half-maximum of the XRD peaks according to Eq. (1) for ZnO and Ag⁺ doped ZnO samples

3.5. Photodegradation experiments of dye.

The experiments are carried out in the photoreactor (phocat 120.0) with 100 ml dye solutions are stirred under ambient conditions in dark for 30 min after the addition of the photocatalyst to reach the adsorption equilibrium on the surface of the photocatalyst. The suspended solution is irradiated. About 5 ml sample is withdrawn from the solution at time intervals for absorbance measurements at the maximum MG dye absorption wavelength of about 614 nm. The photocatalyst is isolated from the heterogeneous solution by the centrifuge before any absorbance measurement at 4000 rpm for 10 min to completely remove the catalyst particles.

RESULTS AND DISCUSSION

4.1. The effect of the photocatalyst loading

The effect of photocatalyst on the degradation kinetics of MG was investigated by employing different concentrations of photocatalyst for both pure ZnO and Ag⁺ doped ZnO varying from (0.5 to 2 g/l) at constant initial dye concentration (14 ppm). As expected, the photodegradation rate of the MG was found to increase then decrease with the increase in the catalyst concentration. In first the increase in the amount of photocatalyst increases the number of active sites on catalyst surface which in turn increases the number of OH[•] and OH₂[•] radicals cause increase photodegradation rate, but at high concentrations of catalyst happens aggregation of catalyst particles causing a decrease in the number of surface active sites and also causes the scattering light leading to decrease in the passage of irradiation through the sample (i.e. reduce of the photonic flux within the irradiated solution) and the degradation rate will decrease. The results are shown in Table.2 and Fig.4 (A) for pure ZnO and (B) for Ag⁺ doped ZnO. As seen in the Fig, the optimum catalyst loading for pure ZnO and Ag⁺ doped ZnO at (1.5g/l).

Table.2 Effect of photocatalyst loading for pure ZnO and Ag⁺ doped ZnO on the degradation rate constants of MG at (14ppm)

Catalyat loading	K(min ⁻¹) Pure ZnO	K(min ⁻¹) Ag ⁺ doped ZnO
0.5	0.03963	0.18694
1	0.04272	0.21218
1.5	0.06055	0.23364
2	0.04763	0.22348

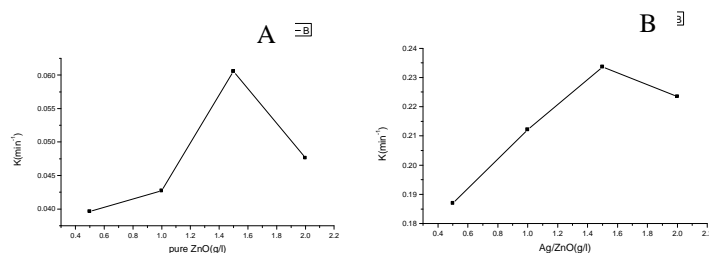


Fig.4. Plot of $K(\text{min}^{-1})$ versus Catalyst loading (A) pure ZnO and (B) Ag^+ doped ZnO for MG dye (14ppm)

4.2. Effect of initial dye concentration

The rate of photodegradation of MG was studied by varying the dye concentration from (12ppm-20ppm) at constant catalyst loading (1.5g/l), the results are shown in Table.3 and Fig. 5 (A) for pure ZnO and (B) for Ag^+ doped ZnO. As seen in the Fig. The degradation is highest at 14 ppm in both pure ZnO and Ag^+ doped ZnO and degradation efficiency is decrease with increase in the dye concentration. This negative effect can be explained as follows; as the dye concentration is increased, the equilibrium adsorption of dye on the catalyst surface active sites increases; hence competitive adsorption of O_2 , H_2O and OH^- on the same sites decreases, meaning a lower formation OH^\bullet radical, which is the principal oxidant necessary for a high degradation efficiency. On the other hand, Considering the Beer-Lambert law, as the initial dye concentration increases, the path length of photons entering the solution decreases, resulting in lower photon adsorption on catalyst particles and, consequently, a lower photodegradation rate.

Table.3 Kinetic rate constant of MG at different dye concentration and catalyst (1.5g/l) for pure ZnO and Ag^+ doped ZnO

concentration of dye	$K(\text{min}^{-1})$ Pure ZnO	$K(\text{min}^{-1})$ Ag^+ doped ZnO
12	0.04019	0.22463
14	0.06055	0.23364
16	0.05271	0.16392
18	0.04779	0.13094
20	0.04099	0.11318

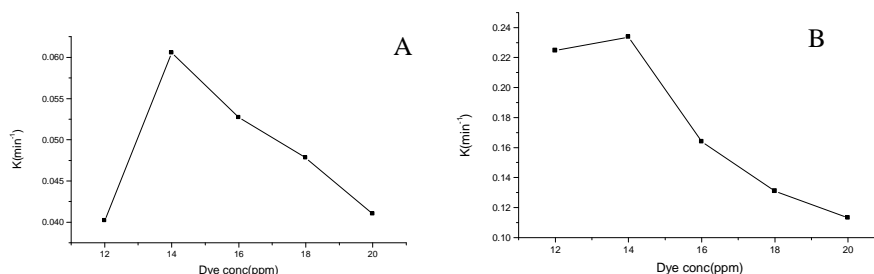
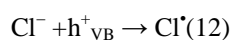
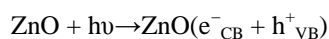


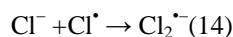
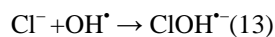
Fig. 5. Plot of $K(\text{min}^{-1})$ versus initial concentrations for MG dye and constant catalyst (A) pure ZnO catalyst (1.5g/l) and (B) Ag^+ doped ZnO catalyst (1.5g/l)

4.3. Effect of Inorganic salts

4.3.1. Effect of NaCl

The occurrence of dissolved inorganic ions is rather common in dye containing industrial wastewater. The role of NaCl on the degradation rate was studied in the range (0.5-2 g/l) for MG dye (14ppm) and catalyst concentration constant (1.5g/l). The results show that the rate of degradation decreases with increasing NaCl concentration for both catalyst, shown in Fig. 6 (A) for pure ZnO and (B) for Ag^+ doped ZnO and in Table.4. Inhibition effects of anions can be explained as the reaction of positive holes and hydroxyl radical with anions, that behaved as h_{vb}^+ and OH^\bullet scavengers (Eqs.(12)–(14)) resulting prolonged color removal. Probably the adsorbed anions compete with dye for the photo-oxidizing species on the surface and preventing the photocatalytic degradation of the dyes [39-41]. Formation of inorganic radical anions (e.g. Cl^\bullet , $\text{ClOH}^{\bullet-}$ and $\text{Cl}_2^{\bullet-}$) under these circumstances is possible to occur [39]





Although the reactivity of these radicals may be considered, they are not as reactive as OH^\bullet due to their lower oxidation potentials [35-37]. Moreover, the presence of radical scavengers (Cl^-) at high doses may retard the advanced oxidation reactions drastically [38].

Table.4 Effect of NaCl concentration on the rate constant of MG dye (14ppm), 1.5g/l for pure ZnO and Ag^+ doped ZnO

Amount of NaCl (g/l)	K(min ⁻¹)Pure ZnO	K(min ⁻¹) Ag^+ doped ZnO
0	0.06055	0.23364
0.5	0.05741	0.12461
1	0.05248	0.11846
2	0.05014	0.10002

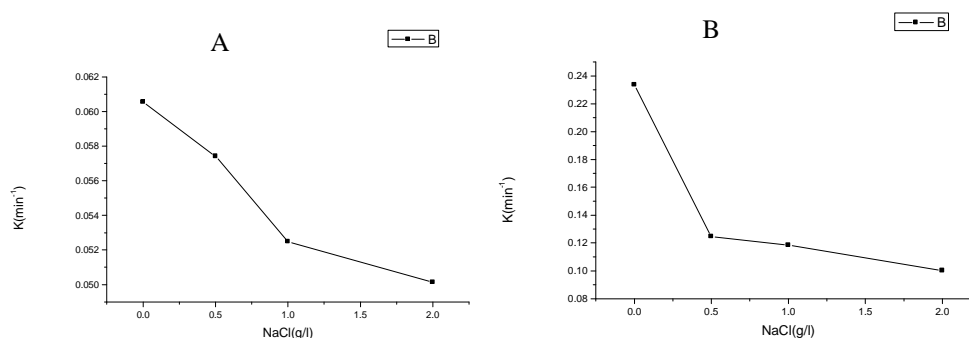
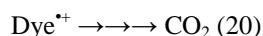
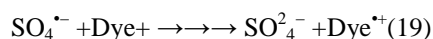
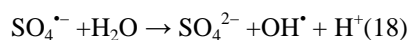
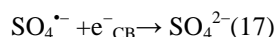
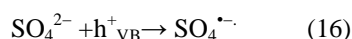
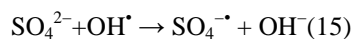


Fig.6. Effect of NaCl concentrations on the rate constant of degradation of MG(14ppm), (A) pure ZnO(1.5g/l) and (B) Ag^+ doped ZnO(1.5g/l)

4.3.2. Effect of Na_2SO_4

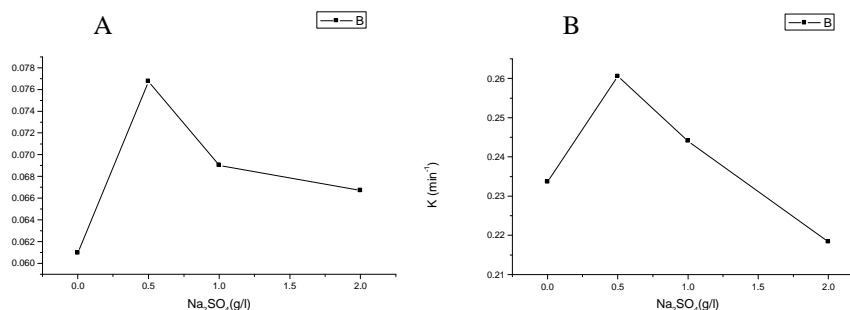
The role of Na_2SO_4 on the degradation rate was studied in the range (0.5-2 g/l) for MG dye (14ppm) and catalyst concentration constant (1.5g/l) for both pure ZnO and Ag^+ doped ZnO. The photodegradation efficiencies were found to increase and then decrease with increasing amount of sulphate ions, show in Fig.7(A) for pure ZnO and (B) for Ag^+ doped ZnO and Table.5. This may be linked to the direct or indirect formation of $\text{SO}_4^{\bullet-}$ chemically shown by Eqs. (15)–(20). Previous literature has shown that this in situ generated radical can sufficiently act as strong oxidising agent or initiate the formation of hydroxyl radical [28,29].



The sulphate radical anion ($\text{SO}_4^{\bullet-}$) thus formed is a very strong oxidant ($E^0 = 2.6\text{eV}$) and may react with dye [44]. It traps the photogenerated electron and/or generates hydroxyl radicals [45]. The hydroxyl radical and sulphate radical anion, being powerful oxidants, degrade the dye molecule. $\text{SO}_4^{\bullet-}$ has the unique tendency to attack dye molecule at various positions and fragment them. Further, the increase in sulphate concentration decreases the degradation rate because adsorbing the excess sulphate ion on the surface of the catalyst and deactivating a section of the catalyst [46].

Table.5Effect of Na₂SO₄ concentration on the rate constant of MG dye (14ppm), 1.5g/l for pure ZnO and Ag⁺ doped ZnO

Amount of Na ₂ SO ₄ (g/l)	K (min ⁻¹) pure ZnO	K (min ⁻¹) Ag ⁺ doped ZnO
0	0.06098	0.23364
0.5	0.07675	0.26052
1	0.06902	0.24402
2	0.06671	0.21834

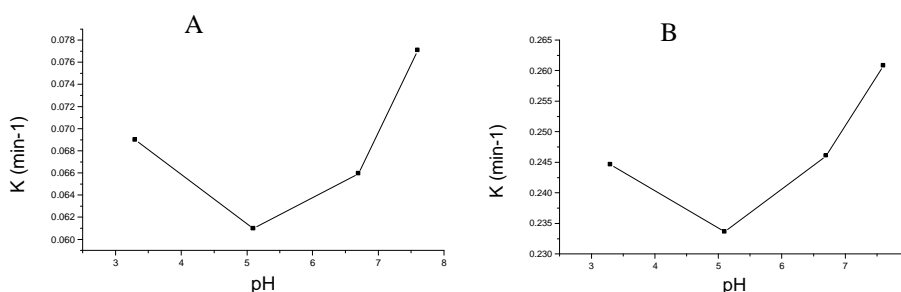
**Fig.7.** Effect of Na₂SO₄ concentrations on the rate constant of degradation of MG(14ppm), (A) for pure ZnO(1.5g/l) and (B) for Ag⁺ doped ZnO (1.5g/l)

4.4. Effect of pH

The waste water from textile industries usually has a wide range of pH values. Further, the generation of hydroxyl radicals is also a function of pH. Thus, pH plays an important role both in the characteristics of textile wastes and generation of hydroxyl radicals. The interpretation of pH effect on the photocatalytic process is very difficult task because of its multiple roles such as electrostatic interactions between the semiconductor surface, solvent molecules, substrate and charged radicals formed during the reaction process. The effect of pH on the photodegradation of MG was studied in the pH range (3.3, 5.1 (aqueous), 6.7 and 7.6) at dye concentration (14ppm) and (1.5g/l) catalyst loading for both pure ZnO and Ag⁺ doped ZnO. The pH of the solution was adjusted before irradiation and was not controlled during the course of the reaction using a dilute aqueous solution of NaOH or H₂SO₄. Show in Fig. 8 (A) for pure ZnO and (B) for Ag⁺ doped ZnO and Table.6. The increase in degradation at pH 3.3 may be influenced by the presence of sulphate ions causes the sulphate radical anion (SO₄^{•-}) formed. The hydroxyl radical and sulphate radical anion (SO₄^{•-}) are powerful oxidant, degrade the dye molecule and degradation efficiency increase. Increasing in pH shows an increasing in degradation efficiency, the presence of a large quantity of OH⁻ ions causes the formation of more OH[•] radicals, which enhances the photocatalytic degradation of MG significantly [44].

Table.6 Effect of pH on the rate constant of M dye (14ppm), 1.5g/l for pure ZnO and Ag⁺ doped ZnO

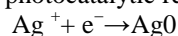
pH	K (min ⁻¹) pure ZnO	K (min ⁻¹) Ag ⁺ doped ZnO
3.3	0.06899	0.24461
5.1	0.06098	0.23364
6.7	0.06594	0.24605
7.6	0.07707	0.26079

**Fig.8:**Effect of pH on the rate constant of degradation of MG(14ppm), (A) for pure ZnO(1.5g/l) and (B) for Ag⁺ doped ZnO (1.5g/l)

4.5. Photocatalytic degradation

The aqueous solutions of methyl green dye (14 ppm) were found to degrade by (37.7%) and (90.9%) on UV-Vis irradiation for 10 min in the presence of the photocatalyst pure ZnO (1.5 g/l) and Ag⁺ doped ZnO (1.5 g/l) respectively, Fig.9. The degradation efficiency of Ag⁺ doped ZnO was found to be much higher than pure ZnO

under similar conditions. In case of pure ZnO the dye was degraded by (85.9%) at 32 min. The photocatalytic activity of ZnO improved by doping with Ag. The enhancing effect of Ag could be clarified by its capability to trap electrons, they perform as electron scavengers. This process decreases recombination of charges and supports oxidation of substrate by producing more OH^\bullet [27]. The reduction effect of silver ion is suitable positioned for active photocatalytic reduction



generating metallic silver on ZnO surface. Thus it was noticed that the catalyst partially darkens during the irradiation [24], and causes increase efficiency of degradation.

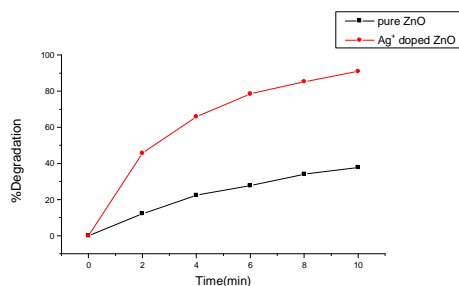


fig.9. Photodegradation of dye using Ag^+ doped ZnO and pure ZnO (1.5g/l) under similar conditions and dye concentration (14ppm) at 10 min

4.6. Water characterizing profile

The water characterizing profile of methyl green dye (14 ppm) aqueous solution showed higher removal efficiencies with using UV-Vis irradiation for 10 min in the presence of the photocatalyst Ag^+ doped ZnO (1.5 g/l) than that obtained from the pure ZnO (1.5 g/l) at the same operating conditions as shown in Table 7. The degradation efficiency of Ag^+ doped ZnO was found to be much higher than pure ZnO under similar conditions in many water quality indicators such as chemical oxygen demand (COD), biological oxygen demand (BOD), pH and temperature. The obtained average COD concentrations by using pure ZnO and Ag^+ doped ZnO were 138 and 101 g/l respectively, with removal efficiencies of 70% and 89% respectively. While those for BOD were 48 and 39 g/l, with removal efficiencies of 78% and 97% respectively. The increasing efficiency of ZnO doped Ag may be explained by its ability to form hydroxyl radicals that are available for chemical decomposition reaction and also can react with organic and/or inorganic substances [4, 24].

Table 7. Water characterizing parameters and efficiencies with using pure ZnO and ZnO doped Ag^+

Parameter	Unit	Raw	Pure ZnO	Efficiency %	ZnO doped Ag^+	Efficiency %
COD	g/l	955	138		101	
BOD	g/l	381	48	70	39	94
pH		5-10	3.3-7.6	78	3.3-7.6	97
Temperature	C°	25-37	20-27		20-37	

CONCLUSION

In the present study, ZnO and Ag^+ doped ZnO nanoparticles have been prepared by Co-Precipitation method. The structure and properties of the resultant materials were characterized by XRD. Ag^+ doped ZnO nanoparticles showed significant improvement in the degradation efficiency of MG dye compared to pure ZnO nanoparticles under UV-Visible light. The removal efficiencies of water quality parameters as COD and BOD were higher in case of Ag^+ doped ZnO, than those obtained from the pure ZnO. The reaction kinetics followed an apparent first-order reaction and was rationalized by a Langmuir–Hinshelwood type mechanism.

The influence of various reaction parameters like effect of pH, catalyst concentration, initial dye concentration and inorganic salt such as Cl^- , SO_4^{2-} were studied and optimum conditions are reported.

REFERENCES

- [1] H. F., Nassar, N., Tang, A., Toriba, F. Kh. Abdel-Gawad, *International Journal of Scientific and Engineering Research (IJSER)*, Volume 6, Issue 8, ISSN 2229 – 5518, August 2015.
- [2] H. F. Nassar, N. Tang, A. Toriba, F. Kh., Abdel-Gawad, G. Guerriero, S. M. Basem, K. Hayakawa, (2015), *IJOAR Journal*. Accepted August 2015.

- [3] F. Kh. Abdel-Gawad, H.F. Nassar, S.M. Bassem, G. Guerriero, W.K.B. Khalil, (2014), *World Applied Sciences Journal* (WASAJ). 12/2014; 32(12):2337-2347. DOI: 10.5829/idosi.wasj.2014.32.12.91175.
- [4] A. A. Abdel-Khalek, H. F. Nassar, F. Kh. Abdel-Gawad, S. M. Basem,., Awad, S. (2016), *Quantum matter*. 5: 1-8.
- [5] C., Ganesh, P., Mongolla, J., Joseph, Maheshwara and V. M., Sarma. *Process Biochem.*, **47**, 1388–1394 (2012).
- [6] Y., Wong and J., Yu. Laccase catalyzed decolourisation of synthetic dye. *Water Res.*, **33**, 3512–3520 (1999).
- [7] Z., Aksu. *Process Biochem.*, **40**, 997–1026 (2005).
- [8] I., Eichlerova, L., Homoika and F., Nerud. *Process Biochem.*, **41**, 941–946 (2006).
- [9] F. d., Duxbury. The photochemistry and photophysics of triphenylmethane dyes in solid and liquid media *Chem. Rev.*, 381-393 (1993).
- [10] J. F., Green. The Sigma–Aldrich Handbook of Stains, Dyes, and Indicators, Aldrich Chemical, Milwaukee, WI, 766 (1990).
- [11] J. K., Lee, J. H. Gu, M. R., Kim and H. S., Chun. *Journal of Chem. Eng.*, **34**, 171-175 (2001).
- [12] J., Garcia-Montano, X., Domenech, A. J., Garcia-Hortal, F., Torrades, and P., Peral. *J. Hazard. Mat.*, **154**, 484-490 (2005).
- [13] W., Chub and W. C., Ma. *Wat. Res.*, **34**, 3153-3160 (2000).
- [14] S. G. A., Prado, M. B., Santos and M. V. G., Jacintho. *Surface Science* **543**, 276 (2003).
- [15] D. J., Torres, E. A., Faria, J. R., Souza and S. G. A., Prado. *J. Photochem. Photobiol.* **182**, 202-206 (2006).
- [16] S. W., Kuo and P. H., Ho. *Chemosphere*. **45**, 77–83. (2001)
- [17] O., Legrini, E., Oliveros and M. A., Braun. *Chem. Rev.* **93**, 671–698 (1993).
- [18] A. M., Behnajady, N., Modirshahla and M., Shokri. *Chemosphere*, **55**, 129–134 (2004).
- [19] R. M., Sohrabi and M., Ghavami. *Desal.*, **252**, 157–162 (2010).
- [20] S., Chakrabarti and B. K., Dutta. *J. Hazard. Mater.* **112**, 269 – 278 (2004).
- [21] A. A., Khodja, T., Sehili, J. F., Pilichowski and J. P., Boule. *J. Photochem. Photobiol.*, **141**, 231-239 (2001).
- [22] N., Daneshvar, D., Salarid and R. A., Khataee. *J. Photochem. Photobiol.*, **162**, 317-322 (2004).
- [23] A. Okasha, F. Gomaa, H. Elhaes, M. Morsy, S. El-Khodary, A. Fakhry and M. Ibrahim, *Spectrochim. Acta A*. **136**, 504-509 (2015).
- [24] B. Dindar and J. S., Icli. *J. Photochem. Photobiol., Chem.*, **140**, 263-268 (2001).
- [25] L. M., Curri, R., Comparelli, P. D., Cozzoli, G., Mascolo and A., Agostiano. *Materials Science and Engineering*, **23**, 285-289 (2003)
- [26] G. J., Yu and X. X., Yu. *Environ. Sci. Technol.*, **42**, 4902-4907 (2008)
- [27] S., Sakthivel, B., Neppolian, V. M., Shankar, B., Arabindoo, M., Palanichamy and V., Murugesan. *Solar Energy Materials and Solar Cells*, **77**, 65-82 (2003).
- [28] S. W., Chiu, S. P., Khiew, M., Cloke, D., Isa, K. T., Tan, S., Radiman, R., Abd-Shukor, M. A., Abd Hamid, M. N., Huang, N. H., Lim and H. C., Chia. *Chem. Eng. J.*, **158**, 345–352 (2010).
- [29] Y. L., Yang, Y. S., Dong, H. J., Sun, L. J., Feng, H. Q., Wu and P. S., Sun. *J. Hazard. Mat.*, **179**, 438–443 (2010).
- [30] H. J., Sun, Y. S., Dong, L. J., Feng, J. X., Yin and C. X., Zhao. *J. Molec. Catal. Chem.*, **335**, 145–150 (2011).
- [28] Z. J., Kong, D. A., Li, Y. X., Li, F. H., Zhai, Q. W., Zhang, P. Y., Gong, H., Li and D., Wu. *J. Solid State Chem.* **183**, 1359–1364 (2010).
- [29] G., Zhou and J., Deng. *Mat. Sci. in Semiconductor Processing*, **10**, 90–96 (2007).
- [29] Y., Zheng, L., Zheng, Y., Zhan, X., Lin, Q., Zheng and K., Wei. *Inorg. Chem.* **46**, 6980–6986 (2007).
- [30] S., Anandan, A., Vinu, P. L. K., Sheeja, N., Gokulakrishnan, P., Srinivasu, T., Moria, V., Murugesan, V., Sivamurugan and K., Ariga. *J. Molec. Catal. Chem.*, **266**, 149–157 (2007).
- [31] A., Mills and L., Hunte. *J. Photochem. Photobiol. Chem.*, **108**, 1–35 (1997).
- [32] O., Carp, L. C., Huisman and A., Reller. *Solid State Chem.* **32**, 33–177 (2004).
- [33] I. K., Konstantinou and A. T., Albanis. *Appl. Catal. Environ.*, **49**, 1–14 (2004).
- [34] K. F., Shan and S. Y., Yu. *J. Eur. Ceram. Soc.* **24**, 1869 (2004).
- [35] C. Z., Tuand X., Hu. *Phys. Rev. B* **74**, 035434 (2006).
- [36] X., Zhou, S., Ge, D., Yao, Y., Zuo and Y., Xiao. *Journal of Alloys and Compounds*, **463**, 9–11 (2008).
- [37] K., Liu, F. B., Yang, H., Yan, Z., Fu, M., Wen, Y., Chen and J., Zuo. *App. Surface Sci.*, **255**, 2052–2056 (2008).
- [38] R., Georgekutty, K. M., Seery and C. S., Pillai. *J. Phys. Chem.*, **112**, 13563-13570 (2008).
- [39] D. R., Shannon and T. C., Prewitt. *Acta Crystallogr. B* **25**, 925 (1989).
- [40] F. Y., Yang, M. M., Al-Jassim and H. S., Wei. *Appl. Phys. Lett.*, **89**, 181912 (2006).
- [41] C., Cheng, G., Xu, H., Zhang, Y., Luo and Y., Li. *Materials Lett.*, **62**, 3733–3735 (2008).
- [42] P. H., Klug and E., Alexander. *X-Ray Diffraction Procedures for Polycrystalline and Amorphous Materials*. Wiley, New York (1984).
- [43] C., Hammond. *The Basic of Crystallography and Diffraction*, Oxford University Press, New York (1997).
- [44] W. D., Bahnemann, J., Cunningham, M. A., Fox, E., Pelizzetti, P., Pichat, N., Serpone, R. G., Heltz and D. G., Crosby. (Eds.), *Aquatic Surface Photochemistry*, Lewis Publishers, Boca Raton . 261 (1994).

- [45] C., Guillard,H.,Lachheb, A.,Houas,M.,Ksibi, E., Elaloui,J.M., Herman. *J. Photochem. Photobiol. A: Chem.*, **158**, 27(2003).
- [46] M.,Sökmen andA., Özkan. *J. Photochem. Photobiol .A: Chem.* **147**, 77-81(2002).